Title
Evidence for spatially variable beam ion diffusion in TFTR

Journal
Plasma Physics and Controlled Fusion, 38(3)

ISSN
0741-3335

Authors
Ruskov, E
Heidbrink, WW
McCune, D
et al.

Publication Date
1996-03-01

DOI
10.1088/0741-3335/38/3/013

Plasma Phys. Control. Fusion **38** (1996) 389–403. Printed in the UK

Evidence for spatially variable beam ion diffusion in TFTR

E Ruskov†, W W Heidbrink†, D McCune‡ and L Johnson‡

†Department of Physics, University of California, Irvine, CA 92717, USA
‡Princeton Plasma Physics Laboratory, Princeton, NJ 08543, USA

Received 25 September 1995, in final form 5 December 1995

Abstract. We present evidence that the fast-ion diffusion coefficient changes across the TFTR plasma column. Two MHD quiescent discharges are analysed: a high power D–T plasma heated with 21 MW of deuterium and tritium beams, and an ohmic plasma into which a 10 MW, 20 ms deuterium beam pulse was injected. The localized charge-exchange measurements in the ohmic plasma, and the neutron flux measurements in the D–T plasma are compared with predictions from the $1\frac{1}{2}D$ transport simulation code TRANSP. We have modified the code to allow modelling with arbitrary fast-ion diffusion profiles $D_f(r)$. Significant improvement in the agreement between measurement and simulation is obtained with a $D_f(r)$ profile that has low values in the inner half of the plasma column ($D_f < 0.05$ m^2 s^{-1}) and then rises rapidly towards the plasma periphery. This suggests a common underlying mechanism of enhanced beam ion transport in the two discharges, such as stochastic ripple diffusion.

1. Introduction

Good confinement of fast ions is essential for fusion energy production in tokamak reactors. The 3.5 MeV alphas from the d(t, n)^{4}He nuclear reaction sustain the burning of the thermal deuterium and tritium. Auxiliary RF and/or neutral beam heating is necessary to ignite the plasma and sustain the toroidal current. The enhanced fast-ion transport decreases the efficiency of each of these processes. The localized expulsion of fast ions is of particular concern because it creates hot spots on the machine walls with possibly disastrous consequences.

Fast ions are usually much better confined than the thermal plasma. This is attributed to finite gyro-radii effects and particle drifts [1, 2]. However, the presence of strong MHD activity or large deviations in the magnetic field symmetry can cause substantial fast-ion losses [3]. For example, in DIII–D plasmas with strong Alfvén eigenmodes, up to 70% of the beam ions were lost from the plasma [4], while in JET, when the field ripple was increased from 1% to 12.5%, the confinement of 1 MeV tritons fell by 30–60% [5].

The actual fast-ion transport can be diffusive or convective. As a simplification, the transport is often quantified with an effective zero-dimensional diffusion coefficient $\langle D_f \rangle$ [3]. Justification for such a treatment can be found in the fact that most of the fusion reactions take place near the plasma centre, where the confinement is the best, and where most of the plasma energy and neutron production are concentrated. It is reasonable to assume that the strength of the physical process behind the enhanced transport does not change much in this region. In this approach, the spatial variation of the fast-ion transport is a secondary effect that slightly affects global quantities, such as the total neutron emission, but can substantially influence local quantities, such as the collimated neutron flux or the flux of charge-exchanged fast neutrals.

0741-3335/96/030389+15$19.50

Various methods were used to infer the fast-ion diffusion coefficient $\langle D_f \rangle$ in tokamak plasmas. They include measurements of triton burn-up [6, 7], plasma stored energy [8], flux of charge-exchanged fast-ion neutrals [9] and escaping fusion products [10]. These measurements resulted in an estimate $\langle D_f \rangle \cong 0.2$ m^2 s^{-1}, or smaller. Analysis of a set of high power, MHD quiescent D–T plasmas at TFTR set an upper limit $\langle D_f \rangle \leqslant 0.2$ m^2 s^{-1} [11].

In this paper we present evidence that the fast-ion diffusion coefficient changes across the plasma column. The evidence is based on analysis of spatially localized measurements in two quite different discharges: one is produced by injecting short beam pulses into an ohmic plasma (#49113), the other is a high power D–T plasma heated with 21 MW of deuterium and tritium beams (#73457). Both of these discharges were previously analysed using spatially constant diffusion coefficients $\langle D_f \rangle$ [12, 13]. It was found that $\langle D_f \rangle = 0$ fits the central measurements, but not the off-axis data ($r/a = 0.3$–0.6). For the off-axis data, $\langle D_f \rangle \sim 0.1$ m^2 s^{-1} was implied. These observations motivated us to add a spatially variable fast-ion diffusion model to the transport simulation code TRANSP [14, 15]. We report new, self-consistent simulations that fit all available measurements. Profiles that provide best fits have small values of D_f near the magnetic axis ($D_f \lesssim 0.05$ m^2 s^{-1}) and rise to $D_f \gtrsim 0.2$ m^2 s^{-1} in the outer part of the plasma ($r/a \gtrsim 0.5$).

In section 2 these two discharges are described in more detail. Measurement and simulation are compared in section 3 (for #73457) and section 4 (#49113). A survey of possible physical mechanisms for the transport indicates that stochastic ripple transport is the most likely explanation (section 5).

2. Discharges #49113 and #73457

The difference in the nature of the two discharges can be seen in figure 1. Shot #49113 is essentially an ohmic plasma into which 10 MW of deuterium beams are injected for ~20 ms. This 'beam blip' is a tiny perturbation for the thermal plasma: it simply provides a test population of fast particles whose behaviour can be observed on the neutron and charge exchange diagnostics. On the other hand, the two tritium and six deuterium beams in shot #73457 triple the central plasma density, and approximately double the central temperature.

The MHD equilibrium for shot #73457 is shown in figure 2(*a*), and for shot #49113, in figure 2(*b*). The locations of the two $E\|B$ charge-exchange analysers [16] are indicated along with the equilibrium for shot #49113. These mass-resolving charge-exchange neutral particle analysers (CENA) are powerful tools for sampling the distribution of banana-trapped fast ions. Unfortunately, they cannot be used in the presence of strong neutron emission (the CENA were dismantled prior to the D–T operations). Thus, the variation in the radial transport of beam ions in plasmas fuelled with deuterium and tritium beams is inferred from radial measurements of the neutron fluxes. The neutron collimator at TFTR [17] provides data at ten radial positions, but only the fluxes in the central four chords, figure 2(*a*), are useful for this study.

3. High power D–T plasma (#73457)

Discharge #73457 ($I_p = 1.8$ MA, $R = 2.52$ m, $a = 0.87$ m), with a peak fusion power of 2.5 MW, was thoroughly analysed in [11]. It has good neutron sensitivity to fast-ion diffusion modelling due to the large (~40%) content of beam–beam neutrons. The numerous TRANSP simulations with spatially constant fast-ion diffusion coefficients

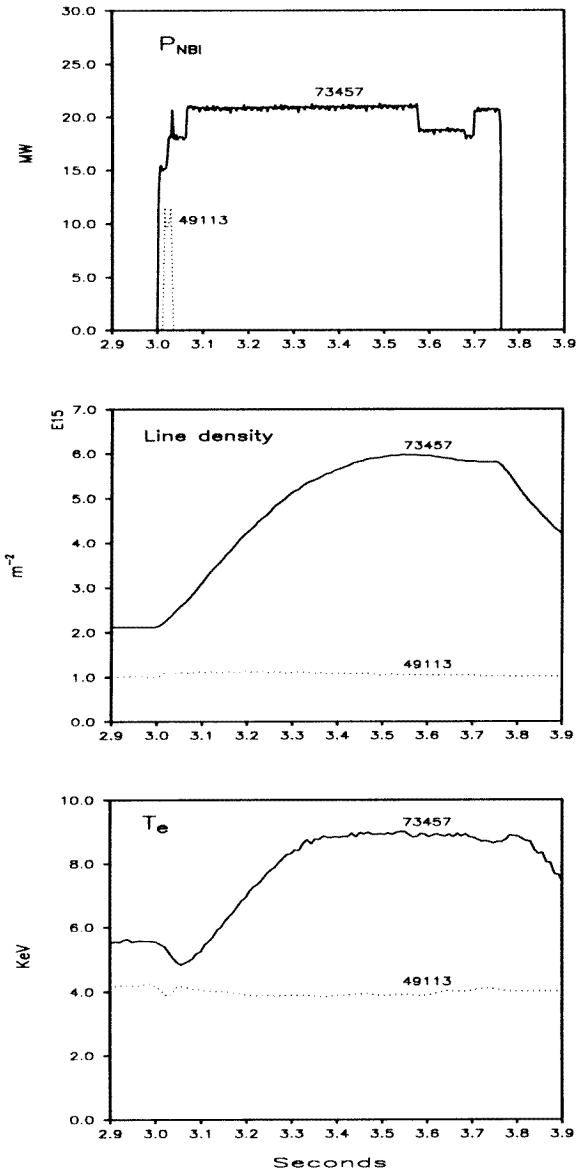

Figure 1. Beam power, line integrated electron density, and electron temperature for the D–T plasma (solid lines) and the beam-blip plasma (dotted lines).

included variations of the input data within their corresponding error bars, and variations in the choice of beam deposition and thermal ion transport models. This systematic error analysis confirmed that $\langle D_{\rm f} \rangle \leqslant 0.2$ m^2 s^{-1}.

We employ an empirical approach in this study. Various trial diffusion profiles are used (figure 3). Our conclusion about the existence of spatially variable fast-ion diffusion in this discharge relies on the neutron flux measurements. The one-sigma uncertainty of these measurements is 12% and its major part can be traced to the uncertainty in the DT

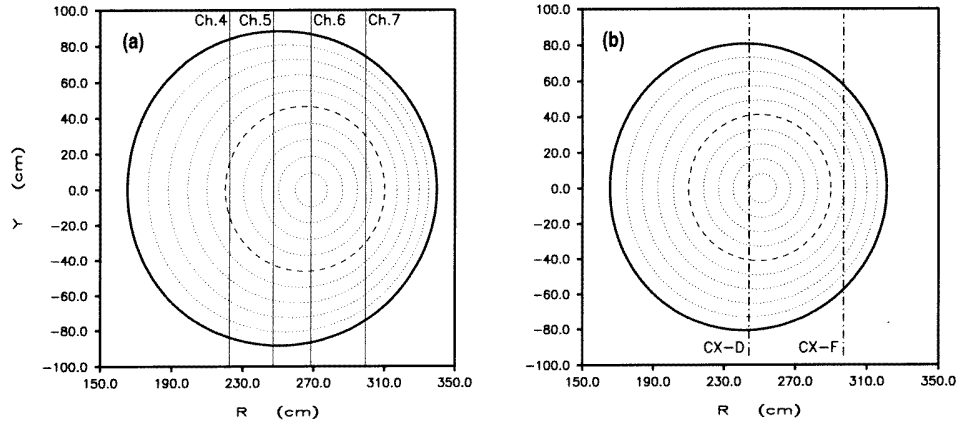

Figure 2. (*a*) MHD equilibrium for shot #73457 at 3.5 s, in the middle of the neutral beam heating interval and the locations of the four central neutron collimator channels. Channel 6 views the very centre of the discharge. The locations of channels 4, 5 and 7 are $R = 222.6$, 247.2 and 299.5 cm, corresponding to flux surfaces $\xi \cong 0.48$, 0.23 and 0.36, respectively. Ten flux surfaces, in increments $\Delta\xi = 0.1$, are shown (dashed line: $\xi = 0.5$ flux surface; solid line: the last closed flux surface; $\xi \equiv \sqrt{(\Psi/\Psi_{\rm lim})}$). (*b*) MHD equilibrium for shot #49113 at 3.0 s, just before the D-beam pulse was injected, and the locations of the two mass-resolving, $E\|B$ charge-exchange chords. For detector EV4, R_{CX-D}=244 cm ($\xi \cong 0.1$) and for detector EV6, R_{CX-F}=297 cm ($\xi \cong 0.6$). Data from these chordal measurements are compared with TRANSP predictions.

generator calibration [18]. The volume integrated neutron emissivity, as obtained from the chordal measurements, agrees to within 7% with the fission detector measurement (figure 4(*a*),(*b*), which is within the uncertainty associated with inferring the total emission from a few chordal measurements. This good agreement is a first condition for proceeding towards comparison between measured and simulated neutron fluxes.

Global measurements are compared with several simulations in figure 4. The $\langle D_{\rm f}\rangle = 0$ model reproduces the total neutron emission (figure 4(*a*)) and diamagnetic flux (figure 4(*c*)) measurements very well. The $D_{\rm f}(\xi) = 1.0\ {\rm m}^2\ {\rm s}^{-1}\xi^4$ model reproduces the neutron emission well (figure 4(*b*)) and is within the $\sim 1\sigma$ of measurement error for the diamagnetic flux measurement (figure 4(*d*)). Here ξ is the normalized flux coordinate.The agreement with the other models is poorer. The $\langle D_{\rm f}\rangle = 0.2\ {\rm m}^2\ {\rm s}^{-1}$ model is slightly outside the errors for both the neutron emission and the diamagnetic flux (figure 4(*a*), (*c*)), while the $\langle D_{\rm f}\rangle = 0.5\ {\rm m}^2\ {\rm s}^{-1}$, $D_{\rm f} = 1.0\ {\rm m}^2\ {\rm s}^{-1}\xi^3$ and $D_{\rm f} = 0.5\ {\rm m}^2\ {\rm s}^{-1}\xi$ give poorer fits to both global measurements.

In figures 5 and 6 these profiles are compared with chordal data from the neutron collimator (all neutron flux curves are smoothed over 20 ms for easier comparison). The modelling with constant fast-ion diffusion coefficients indicates that there is no enhanced transport in the plasma centre, figure 6(*a*). Halfway across the plasma column, at $\xi \cong 0.5$, the $\langle D_{\rm f}\rangle = 0.2\ {\rm m}^2\ {\rm s}^{-1}$ model reproduces the measured fluxes much better. Significant improvement in the predictions for all four central neutron collimator channels is achieved with the spatially variable fast-ion diffusion models, figure 5(*b*),(*d*) and figure 6(*b*),(*d*). Particularly good agreement between measurement and simulation is obtained with the $D_{\rm f}(\xi) = 1.0\ {\rm m}^2\ {\rm s}^{-1}\xi^4$ profile.

Several other types of fast-ion diffusion profiles are investigated (figure 3). The ξ^5

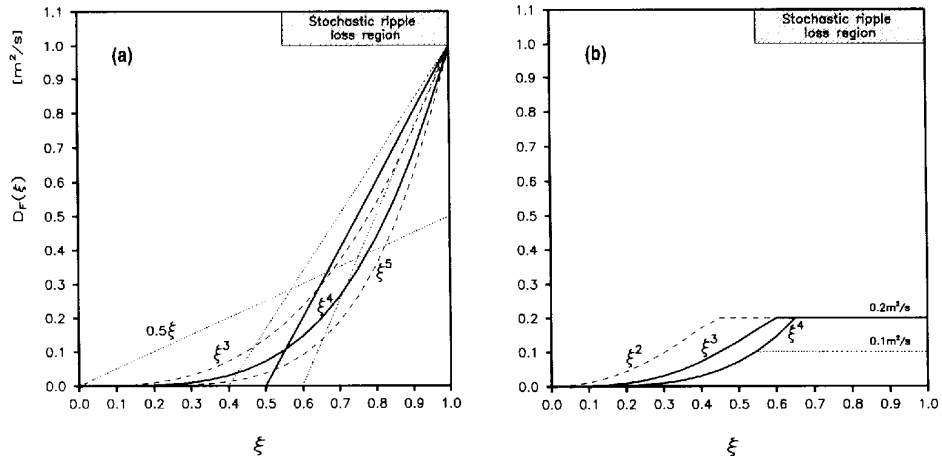

Figure 3. Fast-ion diffusion profiles used in modelling discharges #73457 and #49113. Only neutron flux predictions from models employing the solid line profiles are within the measurement error. The stochastic ripple diffusion region for discharge #73457, considering a deuterium beam ion with $W_\perp = 50$ keV, is shown at the top of these plots.

profile seems to provide fast-ion transport that is too weak: the neutron flux predictions are close to those from the $\langle D_f \rangle = 0$ model. The three linear profiles that start rising at ξ = 0.4, 0.5 and 0.6 are motivated by the threshold character of the stochastic ripple diffusion transport (section 5). It turns out that the profile that starts rising at ξ = 0.4 ($\xi = 0.6$) removes too many (few) fast ions; only the profile that starts rising at ξ = 0.5 predicts neutron fluxes within the measurement error.

Simulations with profiles flattened to a constant value of D_f in the outer plasma column (figure 3(*b*)) are used to check the limits on our conclusions about the physical mechanism behind the enhanced fast-ion transport. The ξ^2 profile flattened to 0.2 m^2 s^{-1} provides transport that is too strong, while the ξ^4 profile flattened to 0.1 m^2 s^{-1}, provides transport that is too weak. The ξ^3 and ξ^4 profiles flattened to 0.2 m^2 s^{-1} predict neutron fluxes within the measurement error. Also, we tried a ξ^4 profile that was forced to drop from 0.15 m^2 s^{-1}, at $\xi \approx 0.6$, to zero, for $\xi > 0.7$ (not shown). The neutron flux predictions indicate that this profile provides transport that is too weak.

The uncertainty in the fast-ion diffusion profiles in the outer plasma column cannot be removed by analysis of the neutron flux data. First, the background noise for channels 1, 2 and 9, 10 is often higher than the measured signal. Second, even if data were available (as for channel 3: $R = 208.5$ cm, $\xi \cong 0.6$, and channel 8: $R = 315.5$ cm, $\xi \cong 0.55$), the neutron fluxes in the outer plasma column are not sensitive to D_f variations, probably because the removal of beam ions from this region is compensated with the arrival of diffusively transported fast ions from the plasma core.

4. Deuterium beam pulse into an ohmic plasma (#49113)

Discharge #49113 ($I_p = 0.79$ MA, $R = 2.42$ m, $a = 0.77$ m) was part of a series of 'beam-blip' experiments performed in the summer of 1990 [12, 19]. We reanalyse this plasma with several spatially constant and variable fast-ion diffusion profiles, using the same assumption that the thermal electron and ion heat diffusivities are the same, as in the

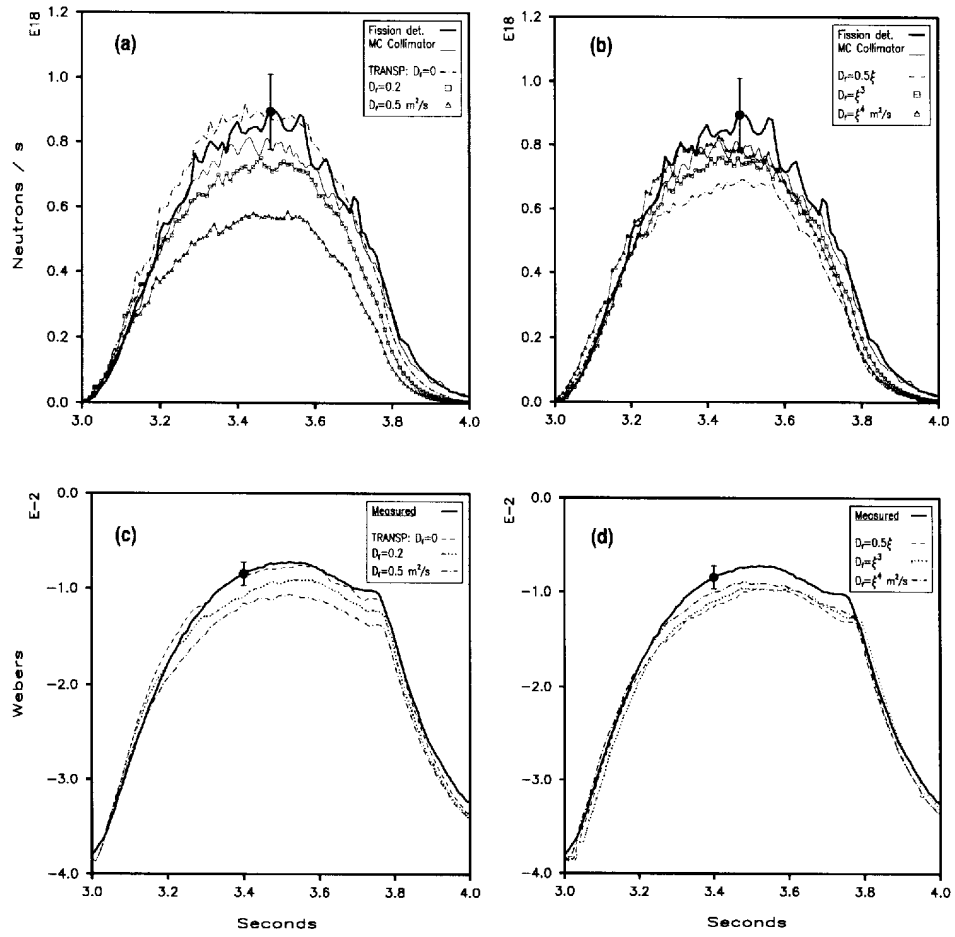

Figure 4. Comparison of the total neutron emission with the TRANSP predictions, (*a*) and (*b*). The integrated neutron emissivity, obtained from the TFTR neutron collimator measurement, is shown together with the fission detector measurement. The measured and the TRANSP predicted diamagnetic flux are compared in (*c*) and (*d*). The error bars are 15% for the neutron emission and 1.2 mW b for the diamagnetic flux measurement.

TRANSP simulations from [12]. The decay rate of the 2.5 MeV neutrons is the only global quantity that is sensitive to these simulations. In addition to models with constant $\langle D_{\rm f}\rangle$ = 0, 0.1, 0.2, 0.5 and 1.0 m^2 s^{-1}, we investigate models with linear profiles: $D_{\rm f}(\xi) = a \cdot \xi$, where a = 0.1, 0.2, 0.5 and 1.0 m^2 s^{-1}, and ξ is the normalized flux coordinate. It turns out that the predictions from the linear models are similar to the models with constant $D_{\rm f}$, provided that $D_{\rm f} = D_{\rm f}(\xi \cong 0.5)$.

Figure 7(*a*) indicates that the overall fast-ion diffusion in this plasma is small: even the $\langle D_{\rm f}\rangle = 0.1$ m^2 s^{-1} prediction is well outside the 15% measurement error bar. The similarity between the decay rates from the models with $\langle D_{\rm f}\rangle = 0.2$ m^2 s^{-1} and $D_{\rm f}(\xi) = 0.5$ m^2 s$^{-1}\xi$ is evident. These two models seem to remove too many beam ions from the plasma centre, where their slowing down time is longer and reactivity higher, resulting in faster neutron emission decay. The ξ^3 and ξ^4 profiles provide much better agreement with the measured

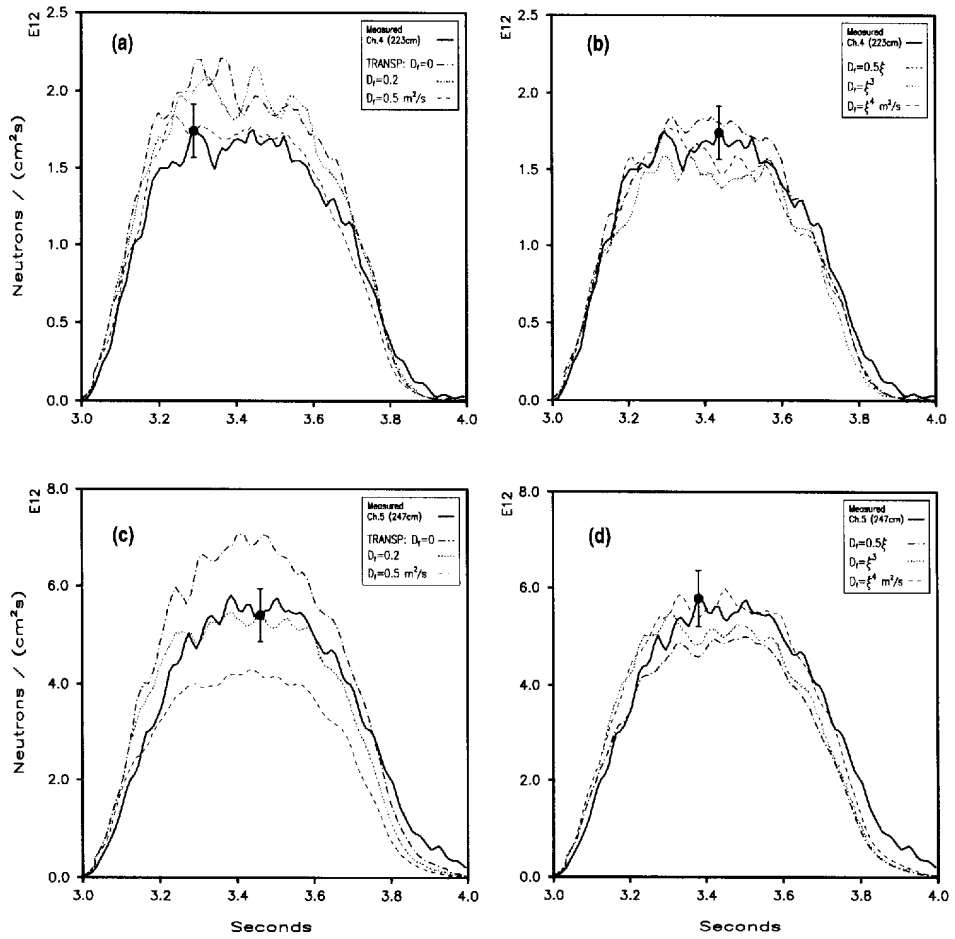

Figure 5. Discharge #73457: comparison of the neutron flux measurements in channels 4 and 5 with TRANSP predictions from three D_f = constant models, (*a*) and (*c*), and three $D_f(\xi)$ models, (*b*) and (*d*). The measured and the TRANSP predicted curves are smoothed over 20 ms. The uncertainty of the measurement is 12% .

decay rate. The critical test about the superiority of the modelling with the ξ^4 profile comes from the analysis of the charge-exchange data, which is the subject of the following subsection.

4.1. Analysis of the charge-exchange data for shot #49113

At the time of this experiment the TFTR neutral beam heating system was delivering ∼48% of the neutrals at $E \cong 90$ keV ('full energy' fraction), ∼28% at $E \cong 45$ keV ('half energy' fraction) and ∼25% at $E \cong 30$ keV ('third energy fraction'). Such a mixture of energies is an inevitable consequence of acceleration of monoatomic, diatomic and triatomic particles in the neutral beam injectors. These neutrals are deposited near the plasma centre, as can be seen from the highly peaked neutron emissivity profiles. The subsequently born

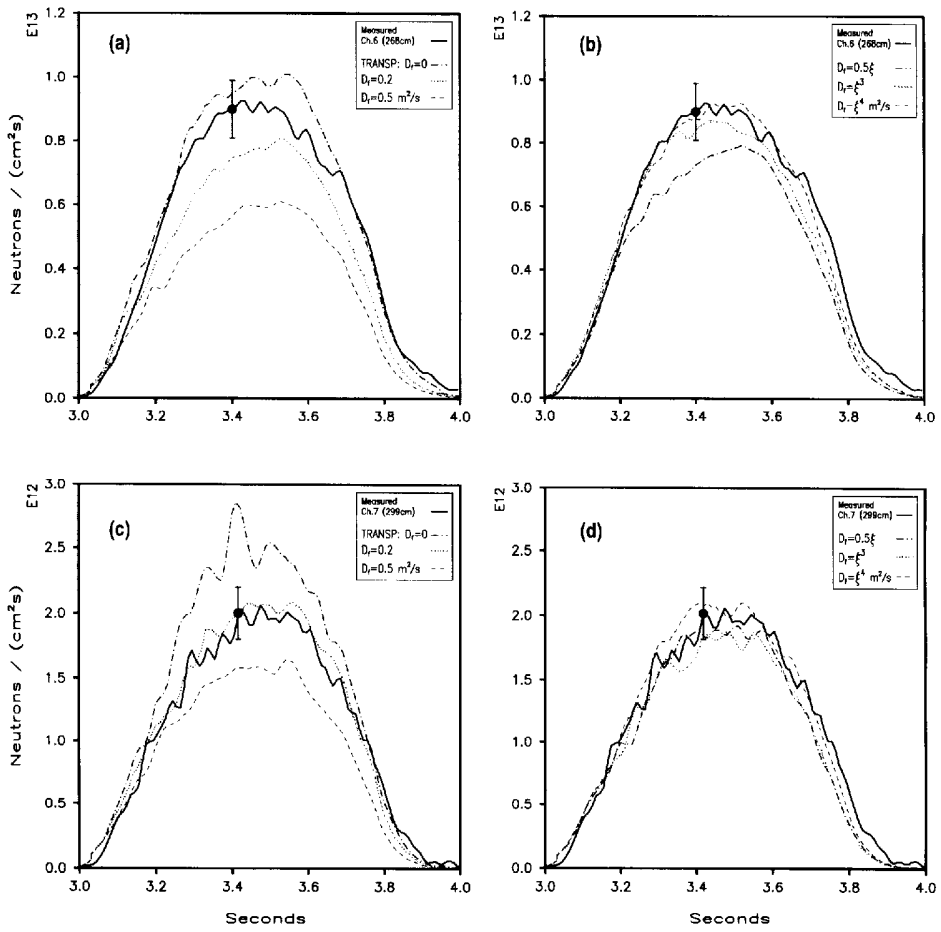

Figure 6. Discharge #73457: comparison of the neutron flux measurements in channels 6 and 7 with TRANSP predictions from three D_f = constant models, (*a*) and (*c*), and three $D_f(\xi)$ models, (*b*) and (*d*). The measured and the TRANSP predicted curves are smoothed over 20 ms. The uncertainty of the measurement is 12%.

fast ions undergo Coulomb collisions which slow them down and scatter them in pitch angle. The slowing down takes place primarily on electrons (for full-energy ions), and strongly depends on the fast-ion energy and the electron temperature: the 90 keV beam ions have a steep profile, while the 30 keV beam ions have almost the same slowing time over the entire plasma column, figure 8. These features are responsible for the characteristics of the measured charge-exchange signals at 50 and 30 keV, along the chords CX–D ($R = 2.44$ m, $\xi \cong 0.1$) and CX–F ($R = 2.97$ m, $\xi \cong 0.6$), figures 9 and 10. The 50 keV signals peak at both chords about 150 ms after the end of the beam pulse, but the reasons for the peaking are quite different. In the plasma centre (chord CX–D) the 90 keV beam ions slow down to 50 keV in ∼150 ms. Halfway across the plasma column (chord CX–F) initially there are many fewer 50 keV ions (the beam deposition is centrally peaked). It takes some kind of a transport process to bring these ions to the radial location of chord CX–F. Assuming that the transport is diffusive in nature, the value of

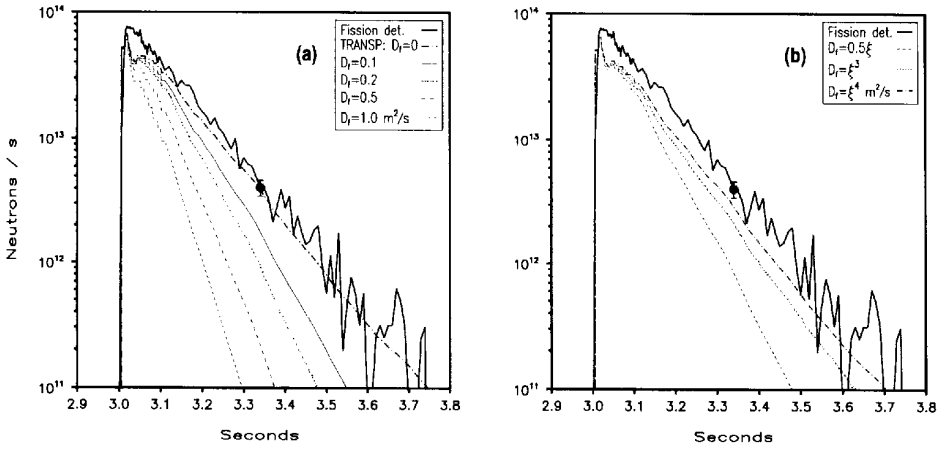

Figure 7. 2.5 MeV neutron emission from a D-beam pulse into an ohmic plasma (discharge #49113). The decay rates from models with constant (*a*) and variable (*b*) fast-ion diffusion profiles are compared with measurements.

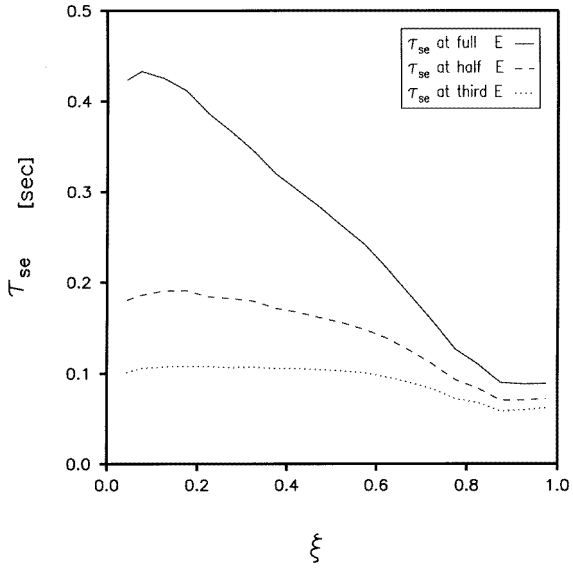

Figure 8. Discharge #49113: classical full (90 keV), half (45 keV) and third (30 keV) energy beam ion slowing down time profiles at the moment when the D-pulse is turned off. Since the pulse is a relatively minor perturbation for the ohmic plasma, these profiles represent the slowing down process of the fast ions well after the D-pulse as well.

the beam ion diffusion coefficient can be determined from a simple random-walk argument: $D_f \cong (\Delta x^2/2\Delta t) = 0.55^2/(2 \times 0.15) = 0.1\ m^2\ s^{-1}$. Figure 9(*c*) clearly shows that the $\langle D_f \rangle = 0$ model cannot match the slower decay time of the measured 50 keV charge-exchange signal at $R = 2.97$ m.

The peaking of the 30 keV signals is different, figure 10, because the half and third energy fraction beam ions also contribute to these signals. The 45 keV beam ions slow

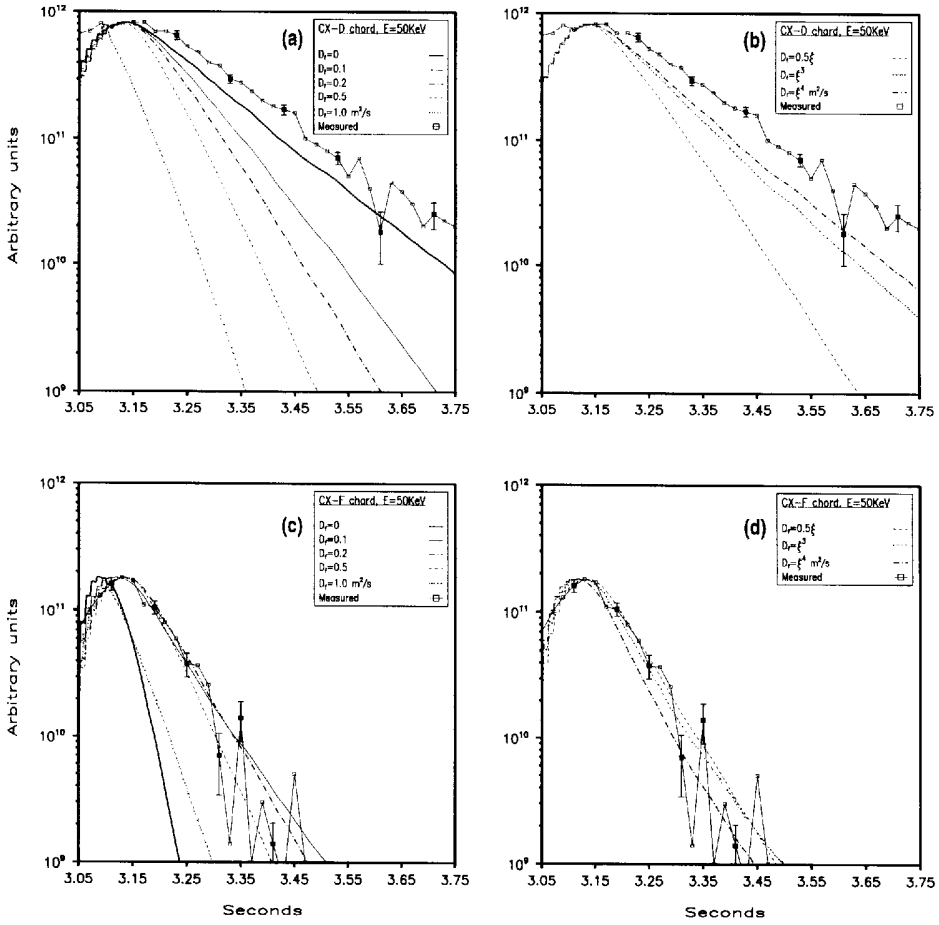

Figure 9. Discharge #49113: charge-exchanged 50 keV deuterium neutrals measured at $R = 2.44$ m (CX–D chord) and $R = 2.97$ m (CX–F chord). Plots (*a*) and (*c*) show comparisons between the experimental data and the predictions from the D_f = constant models. Similar comparisons for the spatially variable fast ion diffusion models are shown in plots (*b*) and (*d*). The TRANSP predictions are normalized to the peak values of the measured signals. The experimental data are obtained by averaging over seven similar D-beam pulses [12]. The error bars are based on counting statistics.

down to 30 keV in ∼50 ms and the signal in chord CX–D starts decaying shortly after the end of the beam pulse. However, the signal in chord CX–F has a constant value for about 120 ms and then decays, the reason being that the full energy beam ions slow down to 30 keV later in time, thus replenishing the lost contribution from the beam ions that slowed down from 45 keV.

We model this plasma with the Fokker–Plank TRANSP option. The Monte Carlo option is not used because noise in the Monte Carlo fast-ion distribution does not allow useful predictions of charge-exchange fast neutral flux. However, both options predict the same total neutron emission.

The D_f = constant models show that the central beam ion diffusion is close to zero

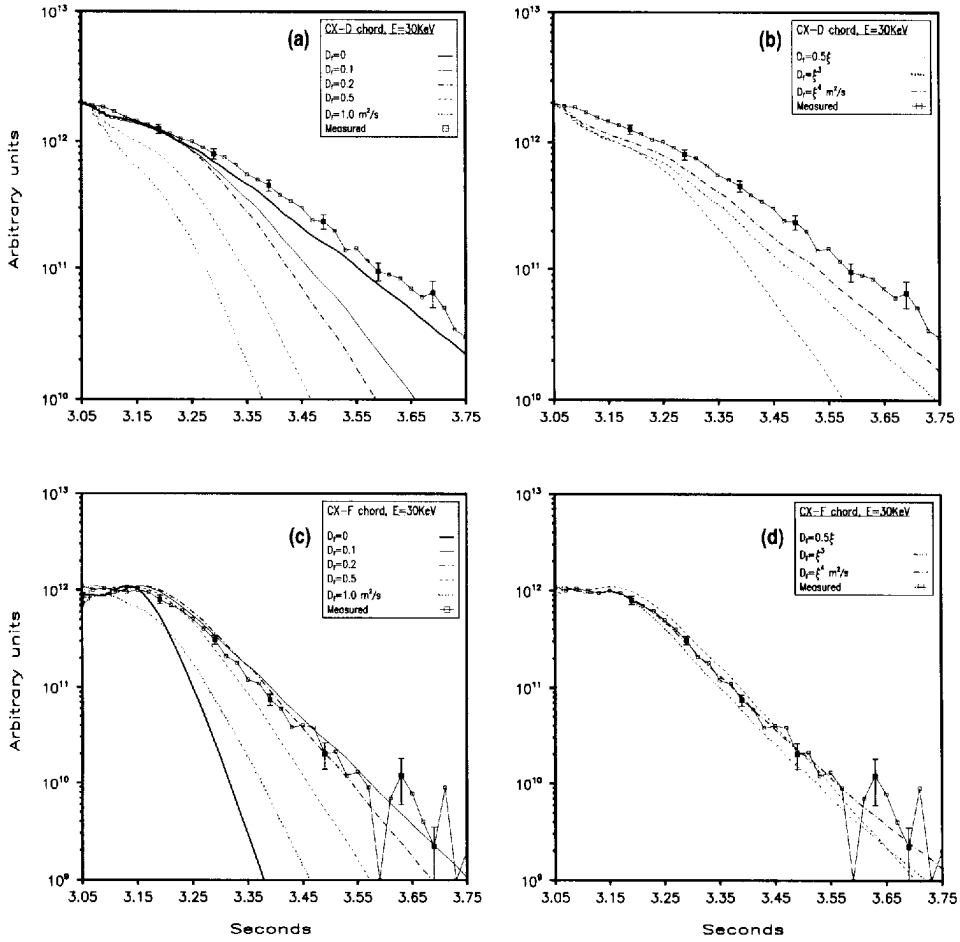

Figure 10. Discharge #49113: charge-exchanged 30 keV deuterium neutrals measured at $R = 2.44$ m (CX–D chord) and $R = 2.97$ m (CX–F chord). Plots (*a*) and (*c*) show comparisons between the experimental data and the predictions from the D_f = constant models. Similar comparisons for the spatially variable fast ion diffusion models are shown in plots (*b*) and (*d*). The TRANSP predictions are normalized to the peak values of the measured signals. The experimental data are obtained by averaging over seven similar D-beam pulses [12]. The error bars are based on counting statistics.

(figures 9(*a*) and 10(*a*)), but the off-axis value is about 0.1–0.2 $m^2\ s^{-1}$ (figures 9(*c*) and 10(*c*)). The increased off-axis diffusion brings more high energy beam ions to the location of chord CX–F, resulting in slower decay than the $\langle D_f \rangle = 0$ prediction. For $\langle D_f \rangle \geqslant 0.5\ m^2\ s^{-1}$, the removal of the beam ions is too strong† and the predicted decay rate is again shorter than the measured one (this is more evident on the 30 keV signal, figure 10(*c*)).

The spatially variable D_f models provide significant improvement in the agreement between the simulations and the measurement, figures 9(*b*), (*d*) and 10(*b*), (*d*). Notice that the $0.5\ m^2\ s^{-1}\xi$ model predicts very similar decay rates as the $\langle D_f \rangle = 0.2\ m^2\ s^{-1}$ model,

† The curves in figure 2(*c*) in [12] are mislabelled: the labels $\langle D_f \rangle = 0$ and $\langle D_f \rangle = 1.0\ m^2\ s^{-1}$ have to be interchanged.

which was already observed for the total neutron decay rates (figure 7). The best fit to the data is achieved with the 1.0 $m^2\ s^{-1}\xi^4$ fast-ion diffusion profile.

The main uncertainty in the TRANSP charge-exchange calculations arises from the unknown neutral deuterium density. There are several sources of deuterium atoms: the halo of neutrals surrounding the beam, the recombination of electrons and ions, the out-gassing of the limiter as it heats up ('cold wall neutrals') and the ions that strike the limiter and re-enter the plasma as neutrals with temperature of approximately the edge T_i or T_e ('warm wall neutrals'). The density of the first three sources is negligible compared with the density of the 'warm wall neutrals'. Since the edge temperature is not known, it is a user-supplied parameter in TRANSP. Hotter neutrals penetrate the plasma deeper and TRANSP tracks their effect on the plasma profiles self-consistently. We tried edge neutral temperatures of 15 eV and 100 eV. The simulation with warmer wall neutrals predicts several times stronger central charge-exchange signals at both 50 keV and 30 keV. However, the decay rates are not affected. The predictions for chord CX–F differ very little both in peak values and in decay rates. These results confirm that the charge-exchange signals depend primarily on the beam ion density and consequently, that the beam ion transport is responsible for their features.

The neutron fluxes in the four central collimator channels were also measured in this discharge [12]. The TRANSP modelling with $D_f(\xi) = 1.0\ m^2\ s^{-1}\xi^4$ agrees well with these data.

5. Discussion

Despite the remarkably different plasma conditions, a similar diffusion profile $D_f = 1.0\ m^2\ s^{-1}\xi^4$ provides the best fit to the fast-ion data for both discharges #73457 and #49113. This suggests that the transport is governed by the same mechanism in both discharges. Neoclassical transport is too small to explain the observations [20].

The deleterious effect of low (m, n) MHD modes on fast-ion confinement is well documented experimentally [3]. Discharge #49113 shows no detectable coherent MHD activity on the magnetic diagnostics; discharge #73457 has an edge Alfvén quasi-coherent mode at ∼200 kHz [21], but no low frequency coherent MHD activity. The sawteeth in discharge #49113 are small [12]; sawteeth are absent during the beam pulse in discharge #73457. Thus, MHD-induced transport of beam ions is an unlikely explanation for the observations.

Microturbulence can also cause fast-ion transport. The expected transport level depends upon details of the microturbulence, which are not well established experimentally. However, if the fluctuations have lengths and velocities that are comparable to the thermal ion gyroradius and speed, the large orbits and speeds of the beam ions effectively average over the turbulence, reducing the predicted transport to a low level [20].

The most likely mechanism of fast-ion transport in these two plasmas is stochastic ripple diffusion [20]. Ripple diffusion affects trapped particles at their banana tips, leading to random drift of the particle orbits. The stochastic ripple diffusion operates in the regions where the local toroidal magnetic field ripple strength δ exceeds a threshold value δ_s given by [22]:

$$\delta \gtrsim \delta_s \equiv \left(\frac{\epsilon}{N\pi q}\right)^{\frac{3}{2}} \frac{1}{(2\rho q')} \tag{1}$$

where ϵ is the inverse aspect ratio, N is the number of toroidal field coils ($N = 20$ for TFTR), ρ is the fast-ion Larmor radius and q and q' are the safety factor and its radial

derivative. The transport increases rapidly towards the plasma periphery.

Experimental evidence for stochastic ripple diffusion and ripple trapping of beam ions at the JT-60U tokamak was provided with infrared cameras [23, 24] and with dedicated experiments using the beam pulse technique [25]. At TFTR, four ZnS(Ag) scintillating detectors located along a poloidal cross section were used in detailed measurements of the escaping 3 MeV protons and 1 MeV tritons from the d(d,p)t fusion reaction [26, 27, 28]. For MHD quiescent discharges these energy, pitch angle and time resolved measurements identified losses in excess of the prompt losses. Analysis of the mid-plane scintillator data confirmed that the transport affected trapped particles only and exhibited a spatially localized threshold [27]. The losses were concentrated just below the mid-plane and were strongly dependent on the plasma current. All these features are signatures of stochastic ripple diffusion.

Ideally, the empirical fast-ion diffusion profiles (figure 3) would be compared with the theoretical ripple diffusion profile†. Since ripple diffusion depends sensitively on fast-ion energy, pitch angle, and spatial position, a one-dimensional D_f that depends only on flux coordinate, such as we have used in our empirical modelling, is not an adequate representation. Thus, we are reduced to simple estimates of the stochastic ripple boundary (equation (1)) and of the magnitude of the expected diffusion. The safety factor q is calculated by the TRANSP code, and the TFTR ripple profile is well known [30]. A deuterium beam ion in discharge #73457, with perpendicular energy $W_\perp = 50$ keV, has a threshold at $\xi \cong 0.55$, figure 3 ($B_T = 5$ T). For deuterium ions with $W_\perp$ in the 40–60 keV range, the threshold spans the $\xi \cong 0.45$–0.65 region. Thus, the region of enhanced spatial diffusion in figure 3 coincides with the expected ripple boundary. The magnitude of the diffusion is also consistent with rough estimates based on 'ripple-plateau' diffusivity [31]. Near the centre of discharge #49113 ($R = 2.5$ m, $z = 0.3$ m), the expected diffusion of 50 keV trapped ions is < 0.01 m^2 s^{-1} while off-axis ($R = 3.0$ m $\Rightarrow \xi \approx 0.7$, $z = 0.3$ m), the calculated ripple diffusion is ~ 0.4 m^2 s^{-1}, which is consistent with our empirical finding that $0.2 \leqslant D_f(\xi = 0.7) \leqslant 0.4$ m^2 s^{-1} (figure 3).

The agreement between the radial location and absolute magnitude of the increased diffusion, together with the observation that two quite different discharges have similar $D_f(r)$ profiles, suggest that ripple diffusion is the probable explanation for the observed fast-ion transport.

6. Conclusions

We analyse localized charge-exchange measurements from a short deuterium beam pulse into an ohmic plasma, and neutron measurements from a high power, reactor-relevant D–T plasma. Transport simulations with spatially variable fast-ion diffusion coefficients provide much better agreement between simulation and measurement than simulations with spatially constant $\langle D_f \rangle$. The diffusion profiles that bring the code predictions within the measurement error suggest that the stochastic ripple diffusion is the probable mechanism for the enhanced fast-ion transport away from the magnetic axis.

In future work, application of this TRANSP analysis technique to a recent set of data [32] that includes systematic variations in plasma position and q profile will further test the hypothesis that ripple diffusion is the dominant transport mechanism. It is also desirable to

† A simple ripple model was recently incorporated into TRANSP [29]. It calculates the stochastic ripple threshold δ_s at each bounce point in the poloidal (R, z) plane and compares it with the toroidal ripple δ. If $\delta > a\delta_s$, where a is an adjustable parameter, the fast ion is declared lost. This model does not include any fast-ion diffusion (only loss), therefore it does not simulate the gradual transport of beam ions outwards.

predict the profile data utilizing the fast-ion distribution function calculated by Monte Carlo [33] or Fokker–Planck [34] codes that include the effects of stochastic ripple diffusion.

Acknowledgments

We are grateful for the assistance of R Budny, G Hammett, L Roquemore and the TFTR team. This work was supported by US DOE contract DE–FG03–92ER5415.

References

[1] Mynick H E and Krommes J A 1979 Particle diffusion by magnetic perturbations of axisymmetric geometries *Phys. Rev. Lett.* **43** 1506
[2] Naitou H, Kamimura T and Dawson J M 1979 Kinetic effects on the convective plasma diffusion and the heat transport *J. Phys. Soc. Japan* 258–65
[3] Heidbrink W W and Sadler G J 1994 The behaviour of fast ions in tokamak experiments *Nucl. Fusion* **34** 535
[4] Duong H H and Heidbrink W W 1993 The confinement of meV ions in DIII-D *Nucl. Fusion* **33** 211
[5] Sadler G *et al* 1992 Effects of enhanced toroidal field ripple on JET plasmas *Plasma Phys. Control. Fusion* **34** 1971
[6] Scott S D *et al* 1991 Local transport measurements during auxiliary heating in TFTR *Proc. 13th Int. Conf. on Plasma Physics and Controlled Nuclear Fusion Research (Washington 1990)* vol I (Vienna: IAEA) pp 235–59
[7] Conroy S, Jarvis O N, Pillon M and Sadler G 1990 A regime showing anomalous triton burnup in JET *Proc. 17th EPS Conf. on Controlled Fusion and Plasma Heating (Amsterdam 1990)* vol 14B (EPS: Petit-Lancy) part I pp 98–101
[8] Cottrell G A and Start D F H 1991 A large-orbit model of fast ion slowing down during ICRH: comparison with JET data *Nucl. Fusion* **31** 61–71
[9] Hawryluk R J *et al* 1991 Overview of TFTR transport studies *Plasma Phys. Control. Fusion* **33** 1509
[10] Zweben S J, Boivin R L, Chang C-S, Hammett G W and Mynick H E 1991 Radial diffusion coefficient for counter-passing MeV ions in the TFTR tokamak *Nucl. Fusion* **31** 2219–2245
[11] Ruskov E, Heidbrink W W and Budny R V 1995 Diffusion of beam ions at the Tokamak Fusion Test Reactor *Nucl. Fusion* **35** 1099
[12] Heidbrink W W *et al* 1991 The diffusion of fast ions in ohmic TFTR discharges *Phys. Fluids B* **3** 3167
[13] Ruskov E, Heidbrink W W and Budny R V 1994 Diffusion of beam ions in TFTR DT plasmas *Workshop on DT experiments (Princeton)* (Princeton, NJ: PPPL) vol 2
[14] Hawryluk R J 1980 An empirical approach to tokamak transport *Physics of Plasmas Close to Thermonuclear Conditions* (Brussels: CEC) vol 1 pp 19–46
[15] Goldston R J 1985 Topics in confinement analysis of tokamaks with auxiliary heating *Basic Physical Processes of Toroidal Fusion Plasmas (Proceedings of Course and Workshop, Varenna)* (Luxemborg: Office for Official Publications of the European Communities) vol 1 pp 165–86
[16] Kaita R, Hammett G W, Gammel G, Goldston R J, Medley S S, Scott S D and Young K M 1988 Measurements with vertically viewing charge exchange analyzers during ion cyclotron range of frequencies heating in TFTR *Rev. Sci. Instrum.* **59** 1691–3
[17] Roquemore A L, Chouinard R C, Diesso M, Palladino R, Strachan J D and Tait G D 1990 TFTR multichannel neutron collimator *Rev. Sci. Instrum.* **61** 3163–5
[18] Jassby D L, Barnes C W, Johnson L C, Roquemore A L, Strachan J D, Johnson D W, Medley S S and Young K M 1995 Absolute calibration by a neutron generator of TFTR neutron detectors for D–T plasma operation *Rev. Sci. Instrum.* **66** 891–3
[19] Kusama Y *et al* 1991 *Technical Report PPPL-2813* Princeton Plasma Physics Laboratory
[20] White R B and Mynick H E 1989 Alpha particle confinement in tokamaks *Phys. Fluids.* B **1** 980
[21] Chang Z *et al* 1995 Alfvén frequency modes at the edge of TFTR plasmas *Technical Report PPPL-3115* Princeton Plasma Physics Laboratory
[22] Goldston R J, White R B and Boozer A H 1981 Confinement of high-energy trapped particles in tokamaks *Phys. Rev. Lett.* **47** 647–9
[23] Tobita K, Neyatani Y, Kusama Y and Takeuchi H 1995 Infrared TV measurements of fast ion loss on JT-60U *Rev. Sci. Instrum.* **66** 594

[24] Tobita K *et al* 1995 Progress in ripple loss studies in JT-60U *4th IAEA Tech. Committee Meeting and Joint US–Japan WS on Alpha Particles in Fusion Research* (Princeton, NJ: PPPL)
[25] Tobita K, Neyatani Y, Kusama Y and Takeuchi H 1994 Fast ion losses due to toroidal field ripple in JT-60U *Nucl. Fusion* **34** 1097–109
[26] Boivin R L, Zweben S J, Chang C S, Hammett G, Mynick H E and White R B 1991 Diffusion of alpha-like MeV ions in TFTR *Proc. 18th European Conf. on Controlled Fusion and Plasma Physics (Berlin 1991)* (Petit-Lancy: EPS) vol 15C part I pp 49–52
[27] Boivin R L, Zweben S J and White R B 1993 Study of stochastic toroidal field ripple losses of charged fusion products at the midplane of TFTR *Nucl. Fusion* **33** 449
[28] Boivin R L and Zweben S J 1993 Midplane measurements of charged fusion product diffusion in the tokamak fusion test reactor *Phys. Fluids.* B **5** 1559
[29] Redi M H *et al* 1995 Modelling TF ripple loss of alpha particles in TFTR DT experiments *Technical Report PPPL-3113* Princeton Plasma Physics Laboratory
[30] Scott S 1990 Princeton Plasma Physics Laboratory, private communication
[31] Goldston R J and Towner H H 1981 Effects of toroidal field ripple on suprathermal ions in tokamak plasmas *J. Plasma Phys.* **26** 283
[32] Zweben S *et al.* 1995 *TFTR Experimental proposal #DT 51* Princeton Plasma Physics Laboratory
[33] Tani K, Takizuka T and Azumi M 1981 *J. Phys. Soc. Japan* **50** 1726
[34] Putvinskij S V, Tubbing B J D, Eriksson L G and Konovalov S V 1994 On the modelling of fast particle ripple losses in tokamaks *Nucl. Fusion* **34** 495